

Supplementary Information

Adjustment of carbon fluxes to light conditions regulates daily turnover of starch in plants: A computational model

Alexandra Pokhilko, Anna Flis, Ronan Sulpice, Mark Stitt, Oliver Ebenhöf

Model description

There are several levels of complexity that need to be considered in order to describe the diurnal regulation of carbon metabolism in plants. Firstly, some reactions are light-dependent and happen only or mainly in presence of light (such as carbon fixation and starch synthesis) or in absence of light (such as starch degradation). Secondly, reactions are compartmentalised between chloroplast (carbon fixation, starch synthesis, the initial steps of starch degradation) and cytosol (sucrose synthesis and the later steps of starch degradation). Thirdly, different sets of reactions prevail in source and sink tissues. Additionally we developed the reactions of the diurnal regulation of carbon fluxes, connected with the circadian clock. Therefore the model consists of 6 blocks of reactions, described in the respective sections below:

A - carbon fixation and starch synthesis; B - starch degradation; C - sucrose synthesis; D - consumption of sucrose by growing sinks; E - diurnal/circadian regulation of carbon metabolism and F - circadian clock itself as a necessary element of the diurnal regulation of metabolism. The units of concentration are mM in our model. For comparison with experimental data, which are mainly presented in g of fresh weight (g FW) or mg of chlorophyll (mg Chl) units the following volume coefficients were used: the stromal volume is assumed to be $v_s=65 \mu\text{l/g FW}=65 \mu\text{l/mg Chl}$, the cytosolic volume $v_c=23 \mu\text{l/g FW}=23 \mu\text{l/mg Chl}$ ^{1,2}. For estimation of parameters and comparison of the model with data we used Arabidopsis data where they were available or other plant's data (mainly spinach). The values of the model parameters are presented in Table S1.

A. Carbon fixation and starch synthesis

In order to decrease the complexity of the whole system, here we developed a minimal model of carbon fixation in the Calvin-Benson cycle (CBC) using a stoichiometric approach to reduce the model to only reactions leading from CO₂ fixation to triose-phosphate export into the cytoplasm, F6P and starch synthesis. This was done using the fact that the kinetics of CBC largely depends on the fluxes of various forms of phosphate in a chloroplast^{3,4}, which are schematically represented on Fig. S1 C. Additionally, similarly to³, we assumed quasi-equilibrium for most of reactions except sFBPase (stromal FBPase) and AGPase, the two key enzymes of starch synthesis⁵. We also included the transport of triose-phosphates between chloroplast and cytosol by triose-phosphate translocator (TPT), which exchanges triose-phosphates with inorganic phosphate (Pi).

All variables of this part of the model are expressed in mM of phosphate units. The reactions of carbon fixation and starch synthesis are combined in equations describing the amount of phosphate groups in the stromal triose phosphates plus F16BP (THP_s); in hexose-phosphates plus AGPG (HP_s); and inorganic phosphate (Pi_s). The equation for starch also includes starch degradation terms and is presented in part E of the Supplementary Information below. THP_s represents a combination of stromal PGA, GAP, DHAP and F16BP; HP_s is a sum of F6P, G6P, G1P and ADPG. The model also includes the variable SP representing the total amount

of phosphate in form of other sugar-phosphates within the CBC (including RuBP). SP is determined from the conservation equation for the total amount of phosphate in the stroma.

The final equations of the CBC are (ordinary differential equations (ODEs) are enumerated):

$$\frac{dTHP_s}{dt} = v_{SP \rightarrow TP} - v_{TP \rightarrow SP} - 2v_{TP \rightarrow HP} - v_{TPT} \cdot \frac{v_c}{v_s} \quad (1)$$

$$\frac{dHP_s}{dt} = v_{TP \rightarrow HP} - v_{HP \rightarrow St} - v_{HP \rightarrow SP} + v_{GPT2} \cdot \frac{v_c}{v_s} \quad (2)$$

$$\frac{dPi_s}{dt} = v_{TPT} \cdot \frac{v_c}{v_s} + v_{HP \rightarrow St} + v_{TP \rightarrow HP} - v_{Pi \rightarrow CBC} - v_{GPT2} \cdot \frac{v_c}{v_s} \quad (3)$$

$$THP_s + HP_s + Pi_s + SP_s = Pi_{tot}$$

$$v_{SP \rightarrow TP} = 3v_{phsyn} \cdot \frac{SP_s}{SP_s + K_{M_SP}}$$

$$v_{TP \rightarrow SP} = \frac{3v_{phsyn}}{2} \cdot \frac{THP_s}{THP_s + K_{M_THP}}$$

$$v_{HP \rightarrow SP} = \frac{v_{phsyn}}{2} \cdot \frac{HP_s}{HP_s + K_{M_HP}}$$

$$v_{Pi \rightarrow CBC} = v_{phsyn} \cdot \frac{Pi_s}{Pi_s + K_{M_ATPsyn}}$$

$$v_{TPT} = v_{TPT_DHAP} + v_{TPT_PGA}$$

Here $v_{TP \rightarrow SP}$, $v_{HP \rightarrow SP}$, $v_{Pi \rightarrow CBC}$ are consumption rates for THP, HP and Pi in the CBC during replenishment of SP. They are determined by the stoichiometry of the CBC (Fig. S1 C) and become limited when concentration of each of the substrates of these reactions drop down; $v_{SP \rightarrow TP}$ is the rate of triose-phosphate formation in the RuBisCO carboxylase reaction of the CBC. It effectively describes the summarised activity of the rate-limiting enzymes of SP replenishment (sedoheptulose biphosphatase, SBPase and ribulose-5-phosphate kinase) and Rubisco; $v_{TP \rightarrow HP}$ and $v_{HP \rightarrow St}$ are the rates of sFBPase and AGPase reactions, respectively, as described below. Additionally we included the GPT2 translocator (v_{GPT2}), exchanging G6P with Pi, which is induced in the chloroplast membrane under stress conditions and described in parts C,E of the Supplementary Information below.

Multiple experimental observations (see, for example ⁶) suggest that the rate of carbon fixation (v_{phsyn}) is constant during the day. At night carbon fixation stops mainly due to redox regulation of reactions in the CBC ⁴. Therefore in the model we assumed that the rate of carbon fixation is expressed as

$$v_{phsyn} = v_{phsyn}^{obs} \cdot L(t),$$

where $L(t)$ is a light function described in part E of the Supplementary Information ($L(t)=1$ when light is on and 0 when it is off) and v_{phsyn}^{obs} is a parameter, which reflects the experimentally observed photosynthesis rate (in CO₂ units per time). The rate of photosynthesis varies depending of the experimental conditions, such as light intensity ⁷. In our model simulations presented here we used a value of v_{phsyn}^{obs} , which corresponds to a moderate light intensity of 150 μmol/m²/s routinely used in labs ⁸⁻¹⁰. The total amount of phosphate in the stroma was estimated as 10 mM based on available data for intermediate

forms of phosphate². Michaelis-Menten constants for $v_{TP \rightarrow SP}$, $v_{HP \rightarrow SP}$, $v_{Pi \rightarrow CBC}$, $v_{SP \rightarrow TP}$ rates were estimated based on the following considerations. For $v_{Pi \rightarrow CBC}$ we assumed that ATP synthase provides the major limitation³. For $v_{TP \rightarrow SP}$, $v_{HP \rightarrow SP}$ we assumed that SBPase is the main limiting enzyme³. Using $K_M=0.013$ mM of SBPase for SBP¹¹ and a ratio of 3.34 of HP to SBP², K_{M_HP} was estimated as 0.04 mM. Similarly, using the observed THP/SBP ratio of 6.32, K_{M_THP} was estimated as 0.08 mM. Parameter K_{M_SP} in $v_{SP \rightarrow TP}$ rate is an effective parameter for the summary of Rubisco and SBPase activities. We varied this parameter to achieve better correspondence with experimentally observed concentrations of stromal metabolites. The chosen value of $K_{M_SP} = 0.6$ mM provided good match with the data. For the rate of sFBPase, which is one of the essentially irreversible steps in the CBC, we used the formula from³, neglecting the small effect of phosphate inhibition compared to F6P:

$$v_{TP \rightarrow HP} = V_{m_sFBP} \cdot \frac{FBP_s}{FBP_s + K_{M_sFBP} (1 + F6P_s / K_{iF6P_FBPase})}$$

For the AGPase rate we also used the formula derived by³ with some minor simplifications under realistic values of stromal ATP and ADP (Table S1 A). With ATP=0.71 mM and ADP=0.23 mM, the rate equation can be expressed as:

$$v_{agpase} = \frac{V_{m_agp} \cdot L(t) \cdot G1P_s \cdot ATP_s}{(G1P_s + K_{M_agp_G1P}) \cdot (ATP_s + K_{M_agp_ATP} (1 + \frac{Pi_s}{K_{a_agp_PGA} (PGA_s + p0)}))}$$

The term $v_{HP \rightarrow St}$ is mainly determined by v_{agpase} . Additionally, $v_{HP \rightarrow St}$ has limitation of starch synthesis rate by high starch levels (described in part E of the Supplementary Information; $v_{HP \rightarrow St} = v_{St_source}$). The small parameter $p0=0.00001$ is introduced to avoid division by 0. AGPase is assumed to be active in presence of light based on the available data¹².

For the export of triose-phosphates we considered only PGA and DHAP, neglecting the small flux of GAP for simplicity. We used the following simple formulation for the rates of TPT:

$$v_{TPT_DHAP} = V_{M_TPT} (DHAP_s \cdot Pi_c - DHAP_c \cdot Pi_s)$$

$$v_{TPT_PGA} = V_{M_TPT} (PGA_s \cdot Pi_c - PGA_c \cdot Pi_s)$$

The rates are expressed in cytoplasmic concentration units, so an additional volume conversion coefficient v_c / v_s , the ratio of cytoplasmic versus stromal volume, is present in the equation for stromal THP (above).

All components of the THP pool were expressed through DHAP based on the rapid equilibrium assumption for intermediate enzymes³:

$$FBP_s = K_{eq_sAld} \cdot GAP_s \cdot DHAP_s$$

$$DHAP_s = K_{eq_TPiso} \cdot GAP_s$$

$$GAP_s \cdot NADP \cdot Pi_s \cdot ADP_s = K_{eq_PGA_GAP} \cdot PGA_s \cdot ATP_s \cdot NADPH$$

and the total phosphate concentration in THP determined by:

$$THP_s = PGA_s + GAP_s + DHAP_s + 2FBP_s$$

The expressions for the components of the THP pool are:

$$GAP_s = DHAP_s / K_{eq_TPiso}$$

$$FBP_s = K_{eq_sAld} \cdot DHAP_s^2 / K_{eq_TPiso}$$

$$PGA_s = \frac{DHAP_s \cdot NADP \cdot Pi_s \cdot ADP_s}{K_{eq_PGA_GAP} \cdot K_{eq_TPiso} \cdot ATP_s \cdot NADPH}$$

$$THP_s = 2K_{eq_sAld} \cdot \frac{DHAP_s^2}{K_{eq_TPiso}} + DHAP_s \cdot \left(1 + \frac{1}{K_{eq_TPiso}} + \frac{NADP \cdot Pi_s \cdot ADP_s}{K_{eq_PGA_GAP} \cdot K_{eq_TPiso} \cdot ATP_s \cdot NADPH}\right)$$

After solving the quadratic equation, the relationship of DHAP to THP pool is determined by:

$$DHAP_s = \frac{\sqrt{b_s^2 + 4a \cdot THP_s} - b_s}{2a}$$

Where

$$b_s = 1 + \frac{1}{K_{eq_TPiso}} + \frac{NADP \cdot Pi_s \cdot ADP_s}{K_{eq_PGA_GAP} \cdot K_{eq_TPiso} \cdot ATP_s \cdot NADPH}$$

$$a = \frac{2K_{eq_sAld}}{K_{eq_TPiso}}$$

Similarly, we related the components of the HP pool using rapid equilibrium assumptions for the intermediate enzymes^{3, 13}:

$$G6P_s = HP_s / (1 + K_{eq_PGM} + 1/K_{eq_PGI})$$

$$F6P_s = HP_s / (1 + K_{eq_PGI} + K_{eq_PGI} \cdot K_{eq_PGM})$$

$$G1P_s = HP_s \cdot K_{eq_PGM} / (1 + K_{eq_PGM} + 1/K_{eq_PGI})$$

The validity of the rapid equilibrium approximation for most of the CBC reactions is justified by the fact that experimentally observed metabolite concentrations are in agreement with the equilibrium conditions^{2, 14}. For a 12L:12D daily cycle the concentrations of stromal metabolites after dawn were: $PGA_s=0.81$ mM; $DHAP_s=0.22$ mM; $GAP_s=0.01$ mM; $FBP_s=0.02$ mM; $G1P_s=0.05$ mM; $G6P_s=0.89$ mM; $F6P_s=0.39$ mM.

We also verified the behaviour of the whole model in the AGPase mutant - the key enzyme of starch synthesis. Two-fold reduction of AGPase activity causes 1.28-fold decrease in starch level, 1.12-fold increase in sucrose level and 1.34-fold increase in the total G6P level after dawn in the model. These results were very close to the experimentally observed 1.3-fold decrease in starch, 1.2-fold increase in sucrose and 1.3-fold increase in G6P in the partial 50% *agpase* mutant¹⁵.

B. Starch degradation

Starch is the main carbon source for plants in darkness. Multiple experiments demonstrated that enzymatic processes of starch degradation are activated on the surface of the starch granule after “lights off”, however the mechanistic details are still unknown^{16, 17}. In our model we simply assumed that starch is degraded only in darkness and multiplied the initial rates of starch degradation by the enzymes β amylase and ISA (isoamylase) by (*I-L*). The corresponding rates are described by the terms $v_{St,\beta am}^M, v_{St,\beta am}^{G3}, v_{St,isa}$ (see below). The final equation for the diurnal kinetics of starch is presented in the part E of the Supplementary Information and it includes starch synthesis in presence of light and its degradation in darkness, which is additionally regulated by the circadian clock through the component α . The starch degradation model component was adopted from^{18, 19}. All parameters were converted from g/L units to glucosyl units, which were used for all intermediate forms of sugars considered in our model: glucose (G), maltose (M), maltotriose (G3), maltopentaose (G5), starch linkage groups (Stlg), which are fragments of the starch polymer released by ISA^{18, 19}. Following¹⁸, starch is initially degraded by β amylase into maltose ($v_{St,\beta am}^M$) or maltotriose ($v_{St,\beta am}^{G3}$). In parallel ISA degrades starch into Stlg ($v_{St,isa}$). Stlg is degraded by β

amylase. Maltotriose enters the disproportionation reaction catalysed by DPE1, releasing glucose and maltopentaose. Although DPE1 catalyses a multitude of other reactions²⁰, the main flux during starch breakdown seems to comprise this reaction. Maltopentaose is further degraded by β amylase. The final products of starch degradation, maltose and glucose, are exported from the chloroplast by MEX1 and GLUT translocators to the cytosol, where maltose is further converted to glucose and G1P by the coordinated action of DPE2 and PHS enzymes. We here neglect the polydisperse intermediates of the soluble heteroglycan pool and describe only the overall reaction, $M + Pi \rightarrow G + G1P$. Finally glucose is phosphorylated by hexokinase and both G6P and G1P enter sucrose synthesis reactions, described in the next section. The equations describing the kinetics of starch degradation are presented below:

$$St_{\beta am} = f \cdot St; St_{isa} = (1 - f) \cdot St$$

$$v_{St,isa} = k_{isa} \cdot (1 - L(t)) \cdot V_{M_isa} \cdot \frac{St_{isa}}{St_{isa} + K_{Misa}}$$

$$v_{St,\beta am}^M = \frac{k_{\beta} \cdot (1 - L(t)) \cdot V_{M_{\beta}} \cdot f_M \cdot St_{\beta am}}{f_M \cdot St_{\beta am} + K_{M\beta}^{St} \left(1 + \frac{M_s^2 + M_s \cdot G3}{K_{Mr}}\right)}$$

$$v_{St,\beta am}^{G3} = \frac{k_{\beta} \cdot (1 - L(t)) \cdot V_{M_{\beta}} \cdot f_{G3} \cdot St_{\beta am}}{f_{G3} \cdot St_{\beta am} + K_{M\beta}^{St} \left(1 + \frac{M_s^2 + M_s \cdot G3}{K_{Mr}}\right)}$$

$$v_{Stlg,\beta am}^M = \frac{k_{\beta}^G \cdot V_{M_{\beta}} \cdot f_M \cdot Stlg}{f_M \cdot Stlg + K_{M\beta}^G \left(1 + \frac{M_s^2 + M_s \cdot G3}{K_{Mr}}\right)}$$

$$v_{Stlg,\beta am}^{G3} = \frac{k_{\beta}^G \cdot V_{M_{\beta}} \cdot f_{G3} \cdot Stlg}{f_{G3} \cdot Stlg + K_{M\beta}^G \left(1 + \frac{M_s^2 + M_s \cdot G3}{K_{Mr}}\right)}$$

$$v_{G5,\beta am} = \frac{k_{\beta}^G \cdot V_{M_{\beta}} \cdot G5}{G5 + K_{M\beta}^G \left(1 + \frac{M_s^2 + M_s \cdot G3}{K_{Mr}}\right)}$$

$$v_{dpe1} = V_{M_dpe1} \cdot \left((G3/3)^2 - \frac{(G5/5) \cdot G_s}{K_{eq}^{dpe}} \right)$$

$$v_{dpe2_phs} = V_{M_dpe2} \cdot \left(M_c / 2 \cdot Pi_c - \frac{G1P_c \cdot G_c}{K_{eq}^{dpe2_phs}} \right)$$

$$v_{mex} = V_{M_mex} \cdot \left(\frac{M_s}{M_s + K_{M_mex}} - \frac{M_c}{M_c + K_{M_mex}} \right)$$

$$v_{glut} = V_{M_glut} \cdot \left(\frac{G_s}{G_s + K_{M_glut}} - \frac{G_c}{G_c + K_{M_glut}} \right)$$

$$v_{hxx} = V_{M_hxx} \cdot \frac{G_c}{G_c + K_{M_hxx} \cdot (1 + G6P_c / K_{iG6P})}$$

$$k_{isa} = g \left(\frac{St_{isa_int}}{St_{tot_int} \cdot (1 - f) + S_0} \right)$$

$$k_{\beta} = g\left(\frac{St_{\beta am_int}}{St_{tot_int} \cdot f + s_0}\right)$$

$$g(x) = 0.5 - a \tan(10 \cdot (x - 1)) / \pi$$

$$St_{tot_int} = St_{\beta am_int} + St_{isa_int}$$

$$\frac{dSt_{isa_int}}{dt} = v_{St,isa} \cdot X - k_{d_int} \cdot L(t) \cdot St_{isa_int} \quad (4)$$

$$\frac{dSt_{\beta am_int}}{dt} = v_{St,\beta am}^M \cdot X + v_{St,\beta am}^{G3} \cdot X - k_{d_int} \cdot L(t) \cdot St_{\beta am_int} \quad (5)$$

$$\frac{dStlg}{dt} = v_{St,isa} \cdot X - v_{Stlg,\beta am}^M - v_{Stlg,\beta am}^{G3} \quad (6)$$

$$\frac{dM_s}{dt} = v_{St,\beta am}^M \cdot X + v_{Stlg,\beta am}^M + 2/5 \cdot v_{G5,\beta am} - v_{mex} \cdot v_c / v_s \quad (7)$$

$$\frac{dG3}{dt} = v_{St,\beta am}^{G3} \cdot X + v_{Stlg,\beta am}^{G3} + 3/5 \cdot v_{G5,\beta am} - 6v_{dpe1} \quad (8)$$

$$\frac{dG_s}{dt} = v_{dpe1} - v_{glut} \cdot v_c / v_s \quad (9)$$

$$\frac{dG5}{dt} = 5v_{dpe1} - v_{G5,\beta am} \quad (10)$$

$$\frac{dG_c}{dt} = v_{glut} + v_{dpe2_phs} - v_{hxx} \quad (11)$$

$$\frac{dM_c}{dt} = v_{mex} - 2v_{dpe2_phs} \quad (12)$$

The indices *c/s* in G and M correspond to cytoplasmic/stromal concentrations of glucose and maltose respectively; v_c / v_s is the ratio of cytoplasmic-to-stromal volumes; *f* and (1-*f*) are fractions of starch degradable by β amylase and ISA and f_M and f_{G3} are fractions of starch degraded to maltose and maltotriose¹⁸; $L(t)$ is a light function described in part E of the Supplementary Information ($L(t)=1$ when light is on and 0 when it is off).

$v_{St,\beta am}^M$, $v_{St,\beta am}^{G3}$ and $v_{Stlg,\beta am}^M$, $v_{Stlg,\beta am}^{G3}$ are rates of maltose and maltotriose formation from starch and starch linkage groups respectively; *X* is a diurnal regulator of starch degradation (described in part E of the Supplementary Information), which modulates the activities of the enzymes, bound to starch granules (β amylase and ISA); $v_{G5,\beta am}$ is a rate of maltopentaose degradation by β amylase; *St* is the total amount of starch; $St_{\beta am}$ and St_{isa} are starch accessible to β amylase and ISA; $St_{\beta am_int}$ and St_{isa_int} are the amount of starch, which was degraded during a night by β amylase and by iso-amylase respectively. These terms are used to regulate the rate constants of β amylase and ISA through the heuristic function $g(x)$. This function, which approaches 0 for increasing argument limits the rate of one of the two enzymes, β amylase or ISA when the relative amount of the product of the other is in excess. Thus, the introduction of this function leads to a constant ratio of activities of β amylase or ISA. The small parameter $S_0=0.01$ is introduced to avoid division by 0. Here we used a similar approach to^{18,19} to describe a competition between β amylase or ISA for starch, but, in contrast to^{18,19}, took into account that starch is insoluble, so the kinetics of starch degradation is regulated by the fraction of the product which was already released from starch

by the corresponding enzyme. The amount of these products $St_{\beta am_int}$ and St_{isa_int} was assumed to fall quickly to negligible levels at the beginning of each day. Similarly to ¹⁸, the expressions for β amylase reaction rates include the term in a denominator for the inhibition by maltose and maltotriose through condensation reactions ²¹. However, we did not consider the reversibility of the β amylase reactions through the condensation reactions because of extremely high K_{eq} (55 M, ¹⁸), which is much higher than the maximal starch concentration in plants (~1 M). Next, the equation for ISA was independent of starch concentration in ¹⁸. This was corrected to avoid reaching negative concentrations of starch by using saturation kinetics with a Michaelis-Menten constant K_{Misa} , which was chosen to be equal to the K_M of β amylase.

The conversion of maltotriose to maltopentaose and glucose by DPE1 in the chloroplast is described similarly to ¹⁸ with the rate v_{dpe1} . Next stages of starch degradation include export of maltose and glucose to the cytosol by MEX1 and GLUT translocators (with rates v_{mex} and v_{glut}). Then maltose is converted to glucose and G1P by DPE2 and PHS reactions (described in one step in our model) with a rate v_{dpe2_phs} . Based on genetic data we assumed that DPE2 is a rate-limiting step in this conversion under physiological conditions ²². Glucose is next phosphorylated by hexokinase in the cytosol and the product of this reaction, G6P, enters sucrose metabolism, further described in the next section (and shown on Fig. 1). Please note that coefficients in equations for starch intermediates reflect the conversion of glucosyl units to concentration units (for example, maltose concentration is equal to M/2, where M is expressed in glucosyl units).

The parameters of the starch degradation reactions are presented in Table S1 B. The maximal rates of β amylase, ISA, MEX1 and GLUT (V_{M_beta} , V_{M_isa} , V_{M_mex} , V_{M_glut}) were varied and chosen to bring the model closer to the experimentally observed levels of starch intermediates in wt at night ²³⁻²⁹.

C. Sucrose synthesis

The model of the sucrose synthesis pathway includes the following steps. Carbon is fixed during the day and exported from chloroplasts to the cytosol by TPT in a form of triose-phosphates (part A of the Supplementary Information, Fig. 1). In the cytosol TP are converted into F1,6P by aldolase or used for glycolysis/respiration (Fig. 1). F1,6P is next directed into the sucrose pathway through the irreversible reaction catalysed by cytosolic FBPase (cFBPase), which produces F6P ^{4,30}. F6P enters a couple of reversible reactions catalysed by the enzymes phosphoglucosomerase PGI, phosphoglucosomutase PGM and UGPase. The final step of sucrose synthesis consists of two coupled enzymes: sucrose-phosphate synthase (SPS) and SPP, which might be considered as one essentially irreversible step resulting in the production of sucrose ^{4,31,32}. Thus the flux of sucrose synthesis is controlled by only two essentially irreversible steps (the first and the last, ⁵): cFBPase and SPS. Cytosolic FBPase is subject to allosteric inhibition by the product F6P and, more strongly, by the specific effector F26P ³³. The F26P level in the cytoplasm is regulated by the bifunctional enzyme F6PK/F26PP, which phosphorylates F6P to produce F26P and dephosphorylates F26P in the reverse reaction. The F26P level is an important regulator of the flux through cFBPase and it is diurnally regulated in parallel with SPS activity ⁴. The coordinated regulation of activity of the enzymes F26PP and SPS (by the function $f_{diurnal}$) is described in part E of the Supplementary Information. Additional to the diurnal regulation, the F26P level is regulated through the allosteric inhibition of F6PK by PGA and F26PP by F6P in the cytoplasm ⁴. In the night G6P and G1P, derived from starch (part B of the

Supplementary Information), bypass cFBPase and enter the same set of reversible reactions as in the day (Fig. 1), which leads to production of sucrose with only SPS controlling the flux at the end of the pathway (Fig. 1; ³¹). To describe the pathway of sucrose synthesis, we introduced a variable THP_c - a total cytosolic pool of trioso-phosphates and F16P. These metabolites are presented in phosphate units in the model and expressed using rapid equilibrium approximation for inter-converting reactions, similar to stromal THP. Cytosolic hexose-phosphates (F6P, G6P, G1P), UDPG, sucrose and F26P are all presented in glucosyl units.

The reactions describing sucrose synthesis are presented below:

$$\frac{dTHP_c}{dt} = v_{TPT} - 2(v_{cFBPase} - v_{PFK}) - v_{resp} \quad (13)$$

$$\frac{dF6P_c}{dt} = v_{cFBPase} - v_{PFK} + v_{PGI} - v_{sps} / 2 \quad (14)$$

$$\frac{dG6P_c}{dt} = v_{HXK} + v_{PGM} - v_{PGI} - v_{GPT2} \quad (15)$$

$$\frac{dG1P_c}{dt} = v_{dpe2_phs} - v_{PGM} - v_{UGPase} \quad (16)$$

$$\frac{dUDPG_c}{dt} = v_{UDPase} - v_{sps} / 2 \quad (17)$$

$$\frac{dsuc_{so}}{dt} = v_{sps} - v_{exp} \quad (18)$$

$$\frac{dF26P_c}{dt} = v_{F6PK} - v_{F26PP} \quad (19)$$

$$v_{PGI} = v_{M_PGI} \cdot (G6P_c / K_{eq_PGI} - F6P_c)$$

$$v_{PGM} = v_{M_PGM} \cdot (G1P_c / K_{eq_PGM} - G6P_c)$$

$$v_{UGPase} = v_{M_UGPase} \cdot \frac{UTP_c \cdot G1P_c - UDPG_c \cdot PPI_c / K_{eq_UGPase}}{UTP_c + K_{M_UTP}}$$

$$v_{SPS} = v_{M_SPS} \cdot f_{diurn}(t) \cdot \frac{F6P_c}{F6P_c + K_{M_F6P}} \cdot \frac{UDPG_c}{UDPG_c + K_{M_UDPG}}$$

$$v_{cFBPase} = v_{M_cFBPase} \cdot \frac{FBP_c}{FBP_c + K_{M_cFBPase} \left(1 + \frac{F6P_c}{K_{iF6P_FBPase}} + \frac{F26P_c}{K_{iF26P}}\right)}$$

$$v_{PFK} = v_{M_PFK} \cdot (PPI_c \cdot F6P_c - Pi_c \cdot FBP_c / K_{eq_PFK})$$

$$v_{F6PK} = v_{M_F6PK} \cdot F6P_c / (F6P_c + K_{M_F6PK} \cdot (1 + PGA / K_{iPGA}))$$

$$v_{F26PP} = v_{M_F26PP} \cdot f_{diurn}(t) \cdot \frac{F26P_c}{F26P_c + K_{M_F26PP} (1 + F6P_c / K_{iF6P_F26PP})}$$

$$v_{resp} = v_{M_resp} \cdot \frac{THP_c}{THP_c + K_{M_resp}}$$

$$THP_c = PGA_c + GAP_c + DHAP_c + 2FBP_c$$

$$GAP_c = DHAP_c / K_{eq_TPiso}$$

$$FBP_c = K_{eq_Ald} \cdot DHAP_c^2 / K_{eq_TPiso}$$

$$PGA_c = \frac{DHAP_c \cdot NADP \cdot Pi_c \cdot ADP_c}{K_{eq_PGA_GAP} \cdot K_{eq_TPiso} \cdot ATP_c \cdot NADPH}$$

$$DHAP_c = \frac{\sqrt{b_c^2 + 4a \cdot THP_c} - b_c}{2a}$$

$$b_c = 1 + \frac{1}{K_{eq_TPiso}} + \frac{NADP \cdot Pi_c \cdot ADP_c}{K_{eq_PGA_GAP} \cdot K_{eq_TPiso} \cdot ATP_c \cdot NADPH}$$

$$a = \frac{2K_{eq_Ald}}{K_{eq_TPiso}}$$

$$v_{GPT2} = v_{M_GPT2} \cdot GPT2(t) \cdot L(t) \cdot (G6P_c \cdot Pi_s - HP_s \cdot Pi_c)$$

v_{PGI} , v_{PGM} , v_{UGPase} , v_{sps} , $v_{cFBPase}$, v_{PFK} , v_{F6PK} , v_{F26PP} describe rates of PGI, PGM, UGPase, SPS, cFBPase, PFK (PPi-dependent phosphofructokinase), F6P kinase, F26P phosphatase reactions, v_{resp} corresponds to the rate of respiration; suc_{so} stands for sucrose concentration in source tissues with the rate of its export to sinks described in the next section. Equations for $G6P_c$ and HP_s , Pi_s (part A of the Supplementary Information) additionally have a term describing GPT2 (v_{GPT2}), the G6P translocator, which exchanges G6P with Pi across the chloroplast membrane. GPT2 activity ($GPT2$) is assumed to be induced only in presence of light under limited carbon condition³⁴, as described in part E of the Supplementary Information. K_{M_resp} for respiration of THP_c was estimated as 0.13 mM based on the Michaelis-Menten constant of 38 μ M for PEP³⁵ and a ratio of 0.3 of PEP to PGA ¹⁰. Equations for hexokinase and DPE2 (producing $G6P_c$ and GIP_c) are presented in part B of the Supplementary Information. The equation for UGPase includes a parameter PPi_c , reflecting the concentration of pyrophosphate, which was estimated to be 0.04 mM based on the fact that UGPase reaction is fast and close to equilibrium and from the measured concentrations of $GIP_c=0.37$ mM, $UDPG_c=5.52$ mM², $UTP_c=1.9$ mM^{4, 36, 37} and K_{eq_UDPase} . The rates of the enzymes F6PK and F26PP (v_{F6PK} , v_{F26PP}) were varied to achieve the observed low concentration of F26P in a range of 4-25 μ M in 12L:12D conditions⁴. The rate of SPS (v_{sps}) was chosen to give the maximum rate of 0.3 mM/s for SPS in 12L:12D^(38, 39); considering the value of $f_{diurn}(t)$ around 1 in 12L:12D). The parameters of all reactions of sucrose synthesis are presented in Table S1 C. The resulting levels of all metabolites correspond to published data^{2, 10, 40}: For a simulated 12L:12D diurnal cycle the metabolite concentrations after dawn are: $G6P_c=7.3$ mM, $F6P_c=3.3$ mM, $GIP_c=0.42$ mM, $UDPG=6.04$ mM, $PGA_c=1.21$ mM, $F16P_c=0.08$ mM, $DHAP_c=0.5$ mM, $F26P_c=13$ μ M. The resulting diurnal profiles of sucrose depend on the photoperiod (Fig. S2 C). “High carbon” level in longer photoperiods increases the demand of carbon by actively growing sinks (D) and decreases the level of carbon stress (I), which both result in a diurnal stimulation of the activity of SPS and cFBPase, via F26PP ($f_{diurn}(t)$; part E of the Supplementary Information). Increased flux through the sucrose synthesis pathway (Fig. 3) elevates sucrose levels in longer days compared to short days (Fig. S2 C). The model also suggests that sucrose kinetics in the *lhy/ccal1* mutant is similar to the wild type during the day, but sucrose falls at the end of the night as a result of starch depletion (Fig. S2 F, Fig. 4).

D. Consumption of sucrose by growing sinks

The source tissues in plants are specialized on the production and export of sucrose, while growing sinks are the main consumers. Young leaves have undetectable level of SPS and high level of starch-degrading enzymes (sucrose-synthase or SuSy and invertase), while mature leaves have high levels of SPS and very low levels of starch-degrading enzymes³². So in a first approximation we can assume that source tissues only export sucrose, while sink tissues only import and consume it. The model presented above in parts A-C of the Supplementary Information describes the process of carbon fixation and storage as a starch, and production of sucrose in source tissues. Here we extend the model by adding reactions of sucrose import and consumption by sinks. We simulated these processes by simply introducing two variables for sucrose (suc_{si}) and a hexose/hexose-phosphate pool (HP_{si}) in sinks, both expressed in glucosyl units. The sucrose is exported from source to sink tissues with a rate v_{exp} ; v_{SuSy} is the rate of sucrose conversion to HP_{si} ³⁰. We assumed that HP_{si} in the sink tissue can be used for both consumption by various processes (v_{cons}) and for the synthesis of starch in sinks (v_{St_sink})^{30, 41}. Equation for v_{St_sink} is presented in part E of the Supplementary Information. Multiple data suggest that a mechanism exists which quickly down-regulates consumption when sucrose level falls down. This happens for example during defoliation (removal) of mature leaves, when sucrose levels initially drop, but are stabilized afterwards⁴². Also in mutants of starch-degrading enzymes (starch-excess or *sex* mutants), which have a reduced flux to sucrose in the night and the sucrose level quickly drops after dusk and then is stabilized^{6, 24, 43}, suggesting a feedback mechanism of down-regulation of consumption by a low carbon status. In the model we assumed the inhibition of consumption by the global sensor of “carbon deficit” I . The equations describing sucrose metabolism in sink tissues are:

$$\frac{dsuc_{si}}{dt} = v_{exp} \cdot V_{so} / (1 - V_{so}) - v_{SuSy} \quad (20)$$

$$\frac{dHP_{si}}{dt} = v_{SuSy} - v_{cons} - v_{St_sink} \quad (21)$$

$$v_{SuSy} = v_{M_SuSy} \cdot (suc_{si} / 2 \cdot UDP_c - HP_{si} \cdot HP_{si} / K_{eq_SuSy})$$

$$v_{exp} = v_{M_exp} \cdot (suc_{so} - suc_{si})$$

$$v_{cons} = v_{M_cons} \cdot HP_{si} \cdot \frac{K_{i_cons}^2}{I^2 + K_{i_cons}^2}$$

Here parameters V_{so} and $(1 - V_{so})$ are the fractional volumes of source and sink tissues, taking values between 0 and 1 both and the total volume is normalised to 1. $V_{so} / (1 - V_{so})$ is the ratio of source-to-sink relative volumes. V_{so} was adjusted to achieve a 3-fold lower level of sucrose in sinks compared to source tissue⁴⁴. Sucrose synthase (SuSy) was assumed to be the main enzyme degrading sucrose to HP_{si} in starch-synthesizing sinks³⁰ for simplicity. The additional effect of invertase in creating the HP_{si} pool (together with hexokinase;³⁰) was accounted for by increasing the parameter v_{M_SuSy} , which effectively reflects the activities of both SuSy and invertase. v_{M_exp} was adjusted to achieve the observed level of sucrose of approximately 40 mM under 12L:12D in source tissues^(4, 6; Fig. S2 C). v_{cons} is diurnally regulated through inhibition by I , described in part E of the Supplementary Information; K_{i_cons} was adjusted to provide a better match to photoperiod data on starch kinetics^{45, 46}.

V_{M_cons} was varied to achieve the maximal starch level of 0.9 M in 12L:12D conditions⁴³.

The parameters of the consumption of sucrose by growing sinks are presented in Table S1 D together with parameters of diurnal regulation in the next section.

E. Diurnal and circadian regulation of carbon metabolism

To describe experimental data on the starch kinetics under varying environmental conditions, we introduced an additional block of equations. They are based on experimental observations, described in more details in Introduction and Materials and Methods. Briefly, starch degradation rate is adjusted according to both starch level at dusk and the time of the dusk in such a way, that starch is almost exhausted at the end of the night in various light conditions⁴⁵; see comments to Fig. S1 B below for more details). Additionally, starch synthesis rate also depends on the duration of the day as described below⁴⁶. To model the adjustment of both starch synthesis and degradation rates to changing light conditions, we introduced two variables, which sense the duration of the day and night respectively: the “timer” α and the “dark sensor” β . Additional to informing the processes of starch synthesis and degradation about environmental conditions such as light/dark, both α and β are regulated by the clock to correct starch turnover according to the time of the day.

The variable β provides the regulation of the global sensor of carbon deficit I according to the current light conditions and the timing of the clock during the day. β is accumulated in darkness to provide a measure of the current level of carbon deficit in our model. This regulation leads to the dynamical adjustment of the level of I , and hence the carbon partitioning and starch synthesis rate as described in Results. The observed changes in starch synthesis rates in clock mutants imply that the regulator of starch synthesis, β , should be modulated by the clock. Dark-dependent accumulation of β results in its dawn peak, which suggested a circadian regulation of β corresponding to dawn genes, which are typically activated by LHY/CCA1 and inhibited by TOC1^{47,48}. Thus we used that type of regulation of β by the clock (see eq. for β below). Interestingly, our analysis of the promoter of AKIN β 1 (At5g21170), a candidate for β , revealed that the promoter has 7 copies of a CCA1 binding site (CBS, AAATCT,⁴⁷) and also 3 copies of G-box-expanded and 2 copies of EE-like expanded binding sites for TOC1⁴⁸, suggesting that the proposed type of the circadian regulation of β corresponds to AKIN β 1, which further suggests AKIN β 1 to be a good candidate for β .

The hypothetical activator of starch degradation α is accumulated during the day and decayed during the night in our model to reflect higher degradation rates of starch in longer days^{46,49}. Thus α is regulated in the opposite manner to β . α stimulates starch degradation through the increase of the level of X as described below.

A number of experiments demonstrate that the rate of starch degradation depends on the starch level and the clock. For example, the “early dusk” experiment, when plants were subject to premature dusk, implies that starch degradation rate is set at dusk according to the starch level (Fig. S1 B). Also experiments with different normal and skeleton photoperiods suggest that starch degradation is set by a timer (α in our model), which measures the time of the day, determined by the circadian clock (Fig. S1 B;⁴⁵).

So we assumed that the starch degradation rate is regulated by α and the starch level through the component X , presumably one of multiple regulatory proteins, capable to bind to the surface of starch granules, such as LSF1 and SEX4^{43,50}. In our model, X is set at dusk by α and the amount of starch. The observed linear rate of starch degradation in most experiments suggests that starch degradation rate might be set once at dusk and does not change much afterwards until starch is almost exhausted. This observation was implemented in the model by increasing X at day time and fixing its level at night. Additional to the

regulation of X by light and the clock, we introduced some inhibition of X by I , based on the observations that plants adapted to long day conditions degrade starch faster than non-adapted plants, which have been transferred from short days⁴⁹. The changes in starch degradation rate under various conditions are also determined by the circadian profile of α . We assumed here that accumulation of α is inhibited by the key clock component LHY/CCA1 (see part F of the Supplementary Information) and activated through a clock-independent mechanism and acute light response, similar to other clock-related morning compounds (such as *PRR9* and *GI*). The acute light response term is described similarly to^{51, 52} through its activation by the light-sensitive activator protein P , a component of the clock model, which is accumulated in the dark and quickly degraded in the light (the equation for P is present in the clock model, see part F of the Supplementary Information). The degradation of α was assumed to be accelerated in darkness and suppressed by the clock element *PRR9* (see eqs. below). The equations for α , β and X are presented below:

$$\frac{dX}{dt} = k_{sX} \cdot \alpha \cdot St \cdot L(t) \cdot (1 + K_{X-I} / (1 + (I / K_{IX-I})^2)) - k_{dX} \cdot L(t) \cdot X \quad (22)$$

$$\frac{d\beta}{dt} = k_{sb,1} \cdot \frac{K_{sb,1}^2}{TOC1^2 + K_{sb,1}^2} + k_{sb,2} \cdot \frac{LHY^2}{LHY^2 + K_{sb,2}^2} - k_{db} \cdot \beta \cdot L(t) \quad (23)$$

$$\frac{d\alpha}{dt} = f_{\alpha+} - f_{\alpha-} \cdot \alpha \quad (24)$$

$$f_{\alpha+} = k_{sa,1} \cdot \frac{K_{sa,1}^2}{LHY^2 + K_{sa,1}^2} + k_{sa,2} + k_{sa,3} \cdot P \cdot L(t)$$

$$f_{\alpha-} = k_{da,1} + \frac{1 - L(t)}{1 + (PRR9 / k_{da,i})^2}$$

The parameters of the equations are presented in Table S1 D. We used Hill coefficient 2 for the effects of clock components TOC1, LHY and *PRR9* since it is known that these proteins work as dimers⁵³⁻⁵⁵. Similarly, Hill coefficient 2 was used for I effect because SnRK1-related kinases dimerize⁵⁶. Parameters were chosen to fit the data on starch time-courses in wild type plants^{43, 46, 49}. Fig. 3 A,B and Fig. S2 A-C show the diurnal profiles of the model components under various photoperiods, under skeleton photoperiod (Fig. S2 D; Fig. S3 B) and in the *lhy/ccal* and *prp7/prp9* mutants (Fig. S2 D-F).

The $L(t)$ is a light function. $L(t)=1$ when light is present, 0 otherwise. To simulate smooth transitions between light and dark, the following light function was used analogous to our previous clock models^{52, 57}:

$$L(t) = 0.5 \cdot ((1 + \tanh((t - period \cdot floor(t / period) - dawn) / T)) - (1 + \tanh((t - period \cdot floor(t / period) - dusk) / T))) + (1 + \tanh((t - period \cdot floor(t / period) - period) / T)))$$

Where *dawn* and *dusk* are the phases of dawn and dusk (normally *dawn*=0); T is the duration of twilight (we used $T=0.05$ h); \tanh and $floor$ – standard functions of hyperbolic tangent and rounding operation; *period* is the duration of the T cycle (normally 24h, except T cycle simulations).

Additionally, we did simulations of the model without metabolic feedback in starch degradation (without the term, which includes I in the equation 22). Although the model without the feedback was capable to reproduce starch kinetics under different photoperiods, the rate of starch degradation in the *lhy/ccal* mutant was too fast compared to the data⁴⁵ (Fig. S3 A). This poor fit to the experimental data is a result of a too strong effect of the clock on the timer of starch degradation α , and hence X (Fig. S3 B,C), which was necessary to describe the drastic increase of the starch degradation rate under long photoperiods in wild-type plants^{49, 58}. The presence of the metabolic feedback allowed us to reduce the clock effect on α

(Fig. 4 C) and hence on starch degradation (Fig. 4 B) compared to the model without feedback (Fig. S3). Moreover, the model without feedback failed to describe the experimentally observed differences in starch levels at dawn between plants subjected to early dusk and plants grown under short photoperiod (Fig. S3 D, compare to Fig. 5 A). Therefore we concluded that the available data correspond better to the model with the feedback via inhibition of starch degradation by I (equation (22)), which was used in all other simulations presented in our paper.

Additionally to starch degradation, starch synthesis rate is also adjusted to changes in the photoperiod in such a way that in short days starch is synthesized faster than in long days and the peak level of starch is nearly constant under various photoperiods⁴⁶. Starch synthesis rate is determined by partitioning of carbon between chloroplasts and cytosol, where triose-phosphates produced during carbon fixation are exported through TPT and next directed to sucrose via coordinated action of cFBPase and SPS (part C of the Supplementary Information; ⁴). Thus the flux to starch is modulated through the change in SPS and cFBPase activities during the day⁴, which are known to be depended on photoperiod⁵⁹. SPS is regulated directly by phosphorylation, while cFBPase is regulated through diurnal modulation of F26PP (part C of the Supplementary Information). An additional mechanism for the regulation of carbon flux in plants was suggested based on the experiments with source/sink manipulations, such as the partial removal of source leaves (defoliation) or applying a petiole block^{32, 42, 60}. These experiments demonstrated that partitioning of carbon to sucrose is up-regulated “on demand” from sink tissues. After the increase in the proportion of growing sinks by such interventions, SPS and cFBPase activities were increased in source leaves, which will presumably support a higher flux through the sucrose synthesis pathway^{42, 60}. Thus we introduced in the model the activation of the SPS and F26PP activities by the demand of the sink tissues for carbon, described by the variable D . The rate of increase in D is set by the rate of carbon consumption by sinks (see below; Fig. S2 A). Higher D elevates SPS and F26PP activities through the term $f_{diurn}(t)$ (below), which also has a ratio of the sink/source volumes to account for the possible changes in the demand upon source/sink manipulations^{42, 60}. Additional to the activation of the flux to sucrose by demand D , SPS and F26PP activities are inhibited in our model by the total level of carbon stress I (see $f_{diurn}(t)$ below), based on experimental observations^{61, 62}.

The total level of carbon deficit is described in our model by the variable I (prototype of SnRK1 activity), which is activated by two levels of “carbon stress”. The first level is related with some minor carbon limitations, which are observed at night under normal carbon-limited conditions, such as short photoperiods or skeleton photoperiods. In this condition there is little of the true starvation response observed (characterized by the induction of starvation marker genes; ⁴⁵). In our model we suggest that activation of β is responsible for this first level of the sensing of carbon limitation during the day and a transfer of this information on the metabolism through the activation of I . Also, I is additionally activated in our model by true starvation conditions, where sugars level drops below a critical threshold K_{i_st} . This was described by increase in I when total sugars and sugar-phosphate level in sink tissues (HP_{si}) falls down (see eq. 25 below). To account for the observed threshold induction of starvation response by sugars drop^{45, 46}, we used high Hill coefficient 3 in equation 25 for I . This additional activation of I occurs when starch reserves are prematurely exhausted before the end of the night, which is the case in wild type in extended night conditions or in some mutants, such as *lhy/ccal*, where markers of carbon starvation are induced^{45, 46}.

Under carbon-limited conditions starch synthesis is also increased through the acute temporal induction of GPT2 translocator in the morning^{34, 63}. The activation of this

translocator of G6P in the chloroplast membrane results in a withdrawal of hexose-phosphates from sucrose to the starch synthesis. This is probably an additional adaptive mechanism, which plants use to accelerate the accumulation of storage resources (starch) and reduce the consumption of carbon for growth in stress conditions. In the model we assumed that GPT2 mRNA is sharply induced (Fig. S2 B), when the amount of carbon deficit I increases above a threshold level (K_{sGPT}) and the activity of GPT2 protein follows its mRNA. The parameters for GPT2 induction were chosen to fit the temporal expression profile of GPT2 mRNA³⁴; Fig 5SA). We used high Hill coefficient 4 to describe threshold induction of GPT2 under carbon-limited conditions. The sharp induction of GPT2 in short days provides better fit of starch timecourses to the photoperiod data, which demonstrate similar peak level of starch under short and normal days⁴⁶. Therefore, absence of GPT2 preferentially affects starch level in shorter days, which is further illustrated with our simulations of a hypothetical *gpt2* mutant on Fig.S6 A.

Finally, the resulting flux to starch synthesis depends: 1) on flux through sucrose synthesis pathway determined by cFBPase and SPS activities through the demand D and the level of carbon deficit I ; 2) on the activity of GPT2, which is determined by the level of carbon deficit through I . The equations for D , I , GPT2 and the diurnal regulation of SPS and F26PP ($f_{diurn}(t)$) are presented below:

$$\frac{dI}{dt} = k_{sl} \cdot \beta \cdot \left(1 - \frac{HP_{si}^3}{HP_{si}^3 + K_{i-sl}^3}\right) - k_{dl} \cdot I \quad (25)$$

$$\frac{dD}{dt} = k_{sD} \cdot v_{cons} - k_{dD} \cdot D \quad (26)$$

$$\frac{dGPT2}{dt} = k_{sGPT} \cdot L(t) \cdot \frac{I^4}{I^4 + K_{sGPT}^4} - k_{dGPT} \cdot GPT2 \quad (27)$$

$$f_{diurn}(t) = \frac{D}{1 + (I / K_{i-diurn})^2} \cdot (1 - V_{so}) / V_{so} + k_{diurn0}$$

All variables in this section (α , β , X , I , D , $GPT2$) are dimensionless. The parameters are presented in Table S1 D below. Parameters of the equations for I , D , $GPT2$, $f_{diurn}(t)$ were chosen to provide better match with the data on starch time-courses in wild type plants^{43, 45, 46}.

The kinetics of starch accumulation is described by the following equation:

$$\frac{St}{dt} = v_{St_source} \cdot V_{so} + v_{St_sink} \cdot (1 - V_{so}) - (v_{St,\beta am}^M + v_{St,\beta am}^{G3} + v_{St,isa}) \cdot X \quad (28)$$

The rate of starch degradation is determined by the rates of β amylase and ISA, as described in part B of the Supplementary Information. Starch degradation rate has an additional term X , related with diurnal regulation. The rate of starch synthesis in source tissues (v_{St_source} , described as $v_{HP \rightarrow St}$ in part A of the Supplementary Information) is presented below. Starch synthesis in sink tissues (v_{St_sink}) is described as follows: we assumed that it is limited only to the illuminated part of the day. The maximal rate of starch synthesis ($V_{M_St_sink}$) was chosen to give a reasonable low amount of starch in sinks (~10%) under 12L:12D conditions, corresponding to levels in mature plants used in our experimental studies. We also assumed, based on GPT2 expression data in the *mex1* and other mutants^{34, 63}, that GPT2 is induced in

both source and sink tissues under carbon-limited conditions. Thus we included an additional term, corresponding to GPT2, into the equation for starch synthesis in sinks (eq. below).

Many datasets suggest that accumulation of starch slows down when the amount of starch exceeds a certain high level (~1M), such as in *sex* mutants or in wild type plants growing under very long days (^{26, 64-66}; Fig. 3 A). The exact mechanism of this limitation of the starch level is unknown, but there is a possibility that there is a physical limitation for the granule size in chloroplasts, which might even lead to the destruction of chloroplasts with excessive amount of starch, such as in the *mex1* mutant ⁶³. So we introduced the limitation of starch synthesis reactions by high concentrations of starch (parameter of this inhibition K_{i_St} was chosen to account for the reasonable levels of starch in starch-excess mutants, such as *lsf1*, Fig. S4 C,D):

$$v_{St_source} = \frac{V_{m_agp} \cdot L(t) \cdot G1P_s \cdot ATP_s}{(G1P_s + K_{M_agp_G1P}) \cdot (ATP_s + K_{M_agp_ATP} (1 + \frac{Pi_s}{K_{a_agp_PGA} PGA_s}))} \cdot \frac{1}{1 + (St / K_{i_St})^2}$$

$$v_{St_sink} = (V_{M_St_sink} + V_{M_GPT2} \cdot GPT2) \cdot L(t) \cdot \frac{HP_{si}}{HP_{si} + K_{St_sink}} \cdot \frac{1}{1 + (St / K_{i_St})^2}$$

The experimental support of the clock's effect on starch metabolism includes data on clock mutants. Thus the kinetics of starch in the *lhy/cca1* mutant is severely perturbed (Fig. 4). Since our model uses the *LHY/CCA1*, *PRRs* and *TOC1* clock genes to regulate α and β , we simulated the effect of the mutation of these genes on starch turnover. The predicted starch-excess profile of the *prr7/prr9* mutant is presented in Results (Fig. 4 D). We also simulated the effect of the *toc1* mutant (Fig. S4 A). Similarly to the data ⁴⁵, the mutation of *TOC1* produces only a minor elevation of the starch level.

Since the component *X* of our model is related with the regulatory proteins on the starch granule, which participate in starch degradation such as LSF1, we simulated the kinetics of the starch-excess mutants, such as the *lsf1* mutant, by reducing the rate constant for the activation of *X*. Fig. S4 C,D shows that the results of our simulations match existing data ⁴³, demonstrating higher levels of starch in the *lsf1* mutant.

One of the key experiments, which demonstrated the importance of the circadian clock in regulating starch diurnal kinetics, is related with varying T cycles (duration of the day) ⁴⁵. The data show the premature depletion of starch at the end of the night in T cycles with 28h duration and an excess of starch at the end of the night in 17h cycles (Fig. S5 B,D). Our model simulations match these data (Fig. S5 A,C) and confirm that the timing of starch degradation is closely linked to the properly functioning clock, which optimizes starch turnover in T cycles close to 24h.

In Results we explored the response of starch metabolism to a variety of environmental perturbations. One of them (Fig. 6), the “early dawn” experiment, introduced weak light 4h before dawn to uncouple the clock from metabolic effects. In this experiment the weak non-photosynthetic light is sufficient to entrain the clock to the new dawn, but not sufficient to affect metabolic responses. To simulate this experiment, we introduced a second light function into the model, which is responsible for light-dependent metabolic changes and not sensitive to the weak non-photosynthetic light. We assumed that all light-dependent metabolic reactions follow this light function, except clock-driven changes in α and the clock

itself, which follow the first light function, which is entrained by the weak light at the end of the night, 4h before dawn (see Results, Fig. 6). The model allowed predicting the diurnal profiles of the unknown component α under “early dawn” conditions (Fig. 6 C).

Another way to explore the properties of the diurnal regulators of starch turnover is to perturb the normal light/dark cycle by introduction of a light pulse during the normal dark period. The model predicts a similar rate of starch degradation in plants unperturbed and perturbed by the night pulse (Fig. S4 E,F), with a corresponding ~5h delay in starch depletion in the “night pulse” experiment due to the starch accumulation during the 5h light pulse⁶⁷.

Effect of AKIN β 1 induction on the starch kinetics

The model suggests that β provides the daily sensing of the light conditions and thus the carbon status, which affects starch synthesis rate. In Results, we present microarray data, which demonstrate that AKIN β 1 is a good candidate for β component of our model (Fig. 7). Next we used the model to explore the effect of AKIN β 1 on the starch timecourse further by simulating an effect of genetical manipulation of AKIN β 1. Since plants possess several β subunits of SnRK1⁶⁸, mutation of only one subunit might be compensated by change in expression of others during plant development. Therefore, the best experiment to verify the role of AKIN β 1 in starch kinetics would be using transient change in expression level of AKIN β 1. Fig.S6 B shows our simulation of the hypothetical transient AKIN β 1-overexpression line. For this simulation we used long day conditions (16L:8D), where AKIN β 1 expression is low in control plant (Fig. 7A). Since AKIN β 1 expressed in the night, we simulated its induction soon after dusk (18ZT) to allow it to reach higher level at the end of the night. The model predicts that increase of AKIN β 1 level should lead to inhibition of the flux to sucrose and increase of starch synthesis rate on the next day after induction (Fig.S6 B).

Parameter stability analysis

In our model we connected the well-defined metabolic blocks of reactions with light and circadian regulation through the small network of the diurnal regulators (I , D , α , β , X , $GPT2$), which orchestrate metabolic fluxes accordingly to the environmental conditions. The structure of the proposed subsystem of the diurnal regulators is partially based on the direct experimental evidence and partially deduced from the observed properties of the starch kinetics as describe above, through multiple intermediate iterations of the model. Most of parameter of this small network are unknown and chosen to fit the existing data as described above. Next we tested the robustness of the model to variation of these parameters. Our analysis showed that simulations, presented in Results, are quite stable against perturbations of the unknown parameters of the diurnal regulators (presented in part D of Table S1). Fig.S7 demonstrates this for the simulated timecourses of starch under three different photoperiods and in the *lhy/cca1* mutant upon 10% changes of each parameter of the equations (22)-(27) for I , D , α , β , X , $GPT2$. From the results presented on Fig.S7 we can conclude that the properties of starch timecourse are only weakly depend on the precise values of parameters. This suggests that the proposed structure of the diurnal regulation is a key determinant of the system behavior.

F. Modelling of the circadian clock in plants

To describe the circadian regulation of α and β , we connect our model to the most recent version of the plant clock⁵², which is schematically presented on Fig. S1 A. The clock

structure consists of interlocked oscillators. The morning loop is based on the autoregulation of the key transcription factors *LHY* and *CCA1* through PRR proteins. The evening loop consists of EC (EVENING COMPLEX) genes *LUX*, *ELF3* and *ELF4*. Both *LHY/CCA1* and EC complexes negatively regulate transcription of multiple target genes⁵⁷. Additionally, the evening protein TOC1 integrates circadian and hormonal (via ABA) information to modulates gene expression⁵².

In summary, our model integrated multiple separate experimental facts into the new concept of the diurnal regulation of carbon metabolism by clock, light and metabolic conditions. The developed separate submodels allowed us to describe carbon fixation in the Calvin-Benson cycle (CBC), sucrose and starch synthesis, starch degradation and consumption of sucrose by sink tissues. Whenever possible we used published models to develop relatively simple modules of carbon metabolism. As such we used a stoichiometric approach to describe the CBC in a way that allowed us to simulate its real-time diurnal kinetics (see^{2,69} for a review on CBC models). We reduced a number of equations to key enzymes and used existing formulations^{3,13}, which were slightly simplified. We also used and simplified some formulations for the enzymes of the sucrose synthesis pathway^{3,13}. Whenever necessary, we added missing important enzymatic steps, not present in existing models. The published model of starch degradation¹⁸ was modified and corrected to adopt the model to the real time-courses of starch and its intermediates and to take into account the insoluble nature of the starch granule. Next we implemented several above-mentioned mechanisms of diurnal regulation, such as regulation of carbon partitioning by the sink's demand (*D*), GPT2 induction and the sensor of carbon deficit *I* (*SnRK1*), which integrates metabolic and circadian (*AKINβ1*) signals, and circadian regulation of starch degradation through the hypothetical clock-related component α . The model allowed to describe and explain multiple experimental observations and predict new experiments to further study and refine the diurnal regulatory mechanisms of starch turnover in plants.

References

1. H. Winter, D. G. Robinson and H. W. Heldt, *Planta*, 1996, **193**, 530-535.
2. A. Arnold and Z. Nikoloski, *Trends Plant Sci*, 2011, **16**, 676-683.
3. G. Pettersson and U. Ryde-Pettersson, *Eur J Biochem*, 1988, **175**, 661-672.
4. M. H. Stitt, S; Kerr, P., in *The Biochemistry of Plants*, eds. M. D. Hatch and N. K. Boardman, Academic Press, New York 1987, vol. 10, pp. 327-409.
5. M. Stitt, J. Lunn and B. Usadel, *Plant J*, 2010, **61**, 1067-1091.
6. S. C. Zeeman and T. A. Rees, ;, *Plant, Cell and Environment*, 1999, **22**, 1445-1453.
7. G. D. Farquhar, S. von Caemmerer and J. A. Berry, *Planta*, 1980, **149**, 78-90.
8. E. T. Pyl, M. Piques, A. Ivakov, W. Schulze, H. Ishihara, M. Stitt and R. Sulpice, *Plant Cell*, 2012, **24**, 2443-2469.
9. A. Strand, R. Zrenner, S. Trevanion, M. Stitt, P. Gustafsson and P. Gardestrom, *Plant J*, 2000, **23**, 759-770.
10. S. Arrivault, M. Guenther, A. Ivakov, R. Feil, D. Vosloh, J. T. van Dongen, R. Sulpice and M. Stitt, *Plant J*, 2009, **59**, 826-839.
11. I. E. Woodrow, D. J. Murphy and D. A. Walker, *Eur J Biochem*, 1983, **132**, 121-123.
12. J. H. Hendriks, A. Kolbe, Y. Gibon, M. Stitt and P. Geigenberger, *Plant Physiol*, 2003, **133**, 838-849.
13. X. G. Zhu, E. de Sturler and S. P. Long, *Plant Physiol*, 2007, **145**, 513-526.
14. J. A. Bassham and G. H. Krause, *Biochim Biophys Acta*, 1969, **189**, 207-221.

15. H. E. Neuhaus, W. P. Quick, G. Siegl and M. Stitt, *Planta*, 1990, **181**, 583-592.
16. A. M. Smith and M. Stitt, *Plant Cell Environ*, 2007, **30**, 1126-1149.
17. S. Streb and S. C. Zeeman, *Arabidopsis Book*, 2012, **10**, e0160.
18. A. Nag, M. Lunacek, P. A. Graf and C. H. Chang, *BMC Syst Biol*, 2011, **5**, 94.
19. F. Shiraishi, K. Kawakami, A. Yuasa, T. Kojima and K. Kusunoki, *Biotechnol Bioeng*, 1987, **30**, 374-380.
20. O. Kartal, S. Mahlow, A. Skupin and O. Ebenhoh, *Mol Syst Biol*, 2011, **7**, 542.
21. E. J. Hehre, G. Okada and D. S. Genghof, *Arch Biochem Biophys*, 1969, **135**, 74-89.
22. J. Fettke, M. Hejazi, J. Smirnova, E. Hochel, M. Stage and M. Steup, *J Exp Bot*, 2009, **60**, 2907-2922.
23. T. Chia, D. Thorneycroft, A. Chapple, G. Messerli, J. Chen, S. C. Zeeman, S. M. Smith and A. M. Smith, *Plant J*, 2004, **37**, 853-863.
24. Y. Lu and T. D. Sharkey, *Planta*, 2004, **218**, 466-473.
25. Y. Lu, J. M. Steichen, S. E. Weise and T. D. Sharkey, *Planta*, 2006, **224**, 935-943.
26. T. Delatte, M. Umhang, M. Trevisan, S. Eicke, D. Thorneycroft, S. M. Smith and S. C. Zeeman, *J Biol Chem*, 2006, **281**, 12050-12059.
27. D. Heineke, A. Kruse, U. I. Flugge, W. B. Frommer, J. W. Riesmeier, L. Willmitzer and H. W. Heldt, *Planta*, 1994, **193**, 174-180.
28. K. Deuschle, B. Chaudhuri, S. Okumoto, I. Lager, S. Lalonde and W. B. Frommer, *Plant Cell*, 2006, **18**, 2314-2325.
29. A. Weber, J. C. Servaites, D. R. Geiger, H. Kofler, D. Hille, F. Groner, U. Hebbeker and U. I. Flugge, *Plant Cell*, 2000, **12**, 787-802.
30. W. P. Quick and A. A. Schaffer, in *Photoassimilate distribution in plants and crops: Source-sink relationships*, eds. E. Zamski and A. A. Schaffer, Marcel Dekker, New York 1996, pp. 115-156.
31. E. MacRae and J. E. Lunn, in *Control of primary metabolism in plants.*, eds. W. C. Plaxton and M. T. McManus, Blackwell Publishing Ltd., Oxford 2006, vol. 22.
32. S. C. Huber, P. S. Kerr and W. Kalt-Torres, in *Phloem transport*, eds. J. Cronshaw, W. J. Lucas, ; and R. G. Giaquinta, Liss, A.R., Inc., New York 1986, pp. 355-367.
33. M. Stitt, *Plant Physiol*, 1987, **84**, 201-204.
34. H. H. Kunz, R. E. Hausler, J. Fettke, K. Herbst, P. Niewiadomski, M. Gierth, K. Bell, M. Steup, U. I. Flugge and A. Schneider, *Plant Biol (Stuttg)*, 2010, **12 Suppl 1**, 115-128.
35. F. E. Podesta and W. C. Plaxton, *Biochim Biophys Acta*, 1992, **1160**, 213-220.
36. R. Zrenner, L. Willmitzer and U. Sonnewald, *Planta*, 1993, **190**, 247-252.
37. I. Ciereszko, H. Johansson and L. A. Kleczkowski, *Biochem J*, 2001, **354**, 67-72.
38. M. Stitt, I. Wilke, R. Feil and H. W. Heldt, *Planta*, 1988, **174**, 217-230.
39. Y. Gibon, O. E. Blaesing, J. Hannemann, P. Carillo, M. Hohne, J. H. Hendriks, N. Palacios, J. Cross, J. Selbig and M. Stitt, *Plant Cell*, 2004, **16**, 3304-3325.
40. R. Gerhardt, M. Stitt and H. W. Heldt, *Plant Physiol*, 1987, **83**, 399-407.
41. P. Niewiadomski, S. Knappe, S. Geimer, K. Fischer, B. Schulz, U. S. Unte, M. G. Rosso, P. Ache, U. I. Flugge and A. Schneider, *Plant Cell*, 2005, **17**, 760-775.
42. T. W. Rufty and S. C. Huber, *Plant Physiol*, 1983, **72**, 474-480.
43. S. Comparot-Moss, O. Kotting, M. Stettler, C. Edner, A. Graf, S. E. Weise, S. Streb, W. L. Lue, D. MacLean, S. Mahlow, G. Ritte, M. Steup, J. Chen, S. C. Zeeman and A. M. Smith, *Plant Physiol*, 2010, **152**, 685-697.
44. T. H. Nielsen and B. Veierskov, *Plant Physiol*, 1990, **93**, 637-641.
45. A. Graf, A. Schlereth, M. Stitt and A. M. Smith, *Proc Natl Acad Sci U S A*, 2010, **107**, 9458-9463.

46. Y. Gibon, O. E. Blasing, N. Palacios-Rojas, D. Pankovic, J. H. Hendriks, J. Fisahn, M. Hohne, M. Gunther and M. Stitt, *Plant J*, 2004, **39**, 847-862.
47. S. L. Harmer and S. A. Kay, *Plant Cell*, 2005, **17**, 1926-1940.
48. W. Huang, P. Perez-Garcia, A. Pokhilko, A. J. Millar, I. Antoshechkin, J. L. Riechmann and P. Mas, *Science*, 2012, **336**, 75-79.
49. Y. Lu, J. P. Gehan and T. D. Sharkey, *Plant Physiol*, 2005, **138**, 2280-2291.
50. S. Janecek, B. Svensson and E. A. MacGregor, *Enzyme Microb Technol*, 2011, **49**, 429-440.
51. J. C. Locke, M. M. Southern, L. Kozma-Bognar, V. Hibberd, P. E. Brown, M. S. Turner and A. J. Millar, *Mol Syst Biol*, 2005, **1**, 2005 0013.
52. A. Pokhilko, P. Mas and A. J. Millar, *BMC Syst Biol*, 2013, **7**, 23.
53. J. S. O'Neill, G. van Ooijen, T. Le Bihan and A. J. Millar, *J Biol Rhythms*, 2011, **26**, 91-98.
54. S. Fujiwara, L. Wang, L. Han, S. S. Suh, P. A. Salome, C. R. McClung and D. E. Somers, *J Biol Chem*, 2008, **283**, 23073-23083.
55. E. Yakir, D. Hilman, I. Kron, M. Hassidim, N. Melamed-Book and R. M. Green, *Plant Physiol*, 2009, **150**, 844-857.
56. R. Ghillebert, E. Swinnen, J. Wen, L. Vandesteene, M. Ramon, K. Norga, F. Rolland and J. Winderickx, *FEBS J*, 2011, **278**, 3978-3990.
57. A. Pokhilko, A. P. Fernandez, K. D. Edwards, M. M. Southern, K. J. Halliday and A. J. Millar, *Mol Syst Biol*, 2012, **8**, 574.
58. Y. Gibon, E. T. Pyl, R. Sulpice, J. E. Lunn, M. Hohne, M. Gunther and M. Stitt, *Plant Cell Environ*, 2009, **32**, 859-874.
59. S. C. Huber, T. W. Rufty and P. S. Kerr, *Plant Physiol*, 1984, **75**, 1080-1084.
60. T. W. Rufty, S. C. Huber and P. S. Kerr, *Plant Science Letters*, 1984, **34**, 247-252.
61. C. Sugden, P. G. Donaghy, N. G. Halford and D. G. Hardie, *Plant Physiol*, 1999, **120**, 257-274.
62. A. Kulma, D. Villadsen, D. G. Campbell, S. E. Meek, J. E. Harthill, T. H. Nielsen and C. MacKintosh, *Plant J*, 2004, **37**, 654-667.
63. M. Stettler, S. Eicke, T. Mettler, G. Messerli, S. Hortensteiner and S. C. Zeeman, *Mol Plant*, 2009, **2**, 1233-1246.
64. T. Niittyla, G. Messerli, M. Trevisan, J. Chen, A. M. Smith and S. C. Zeeman, *Science*, 2004, **303**, 87-89.
65. O. Kotting, D. Santelia, C. Edner, S. Eicke, T. Marthaler, M. S. Gentry, S. Comparot-Moss, J. Chen, A. M. Smith, M. Steup, G. Ritte and S. C. Zeeman, *Plant Cell*, 2009, **21**, 334-346.
66. J. H. Critchley, S. C. Zeeman, T. Takaha, A. M. Smith and S. M. Smith, *Plant J*, 2001, **26**, 89-100.
67. A. Scialdone, S. T. Mugford, D. Feike, A. Skeffington, P. Borrill, A. Graf, A. M. Smith and M. Howard, *Elife*, 2013, **2**, e00669.
68. C. Polge, M. Jossier, P. Crozet, L. Gissot and M. Thomas, *Plant Physiol*, 2008, **148**, 1570-1582.
69. J. Jablonsky, H. Bauwe and O. Wolkenhauer, *BMC Syst Biol*, 2011, **5**, 185.

Figures

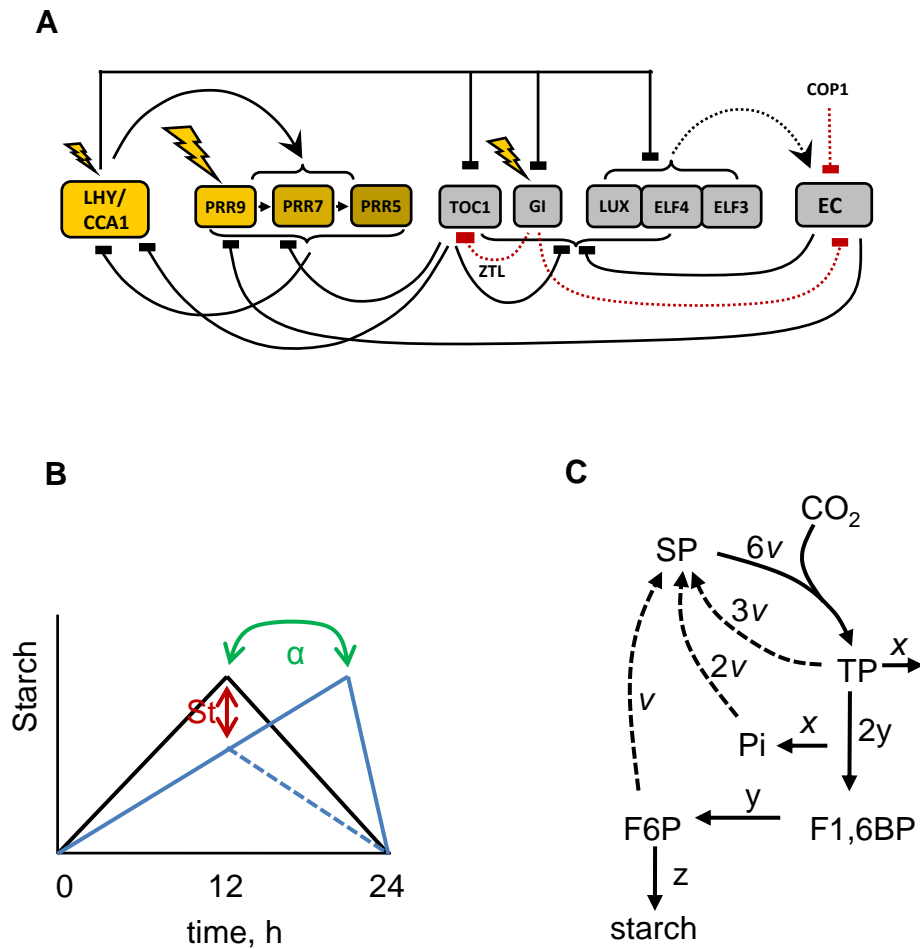


Figure S1. Schematic representation of the main principles of regulation of the CBC and starch degradation in the model and a diagram of the most recent circadian clock model. **A.** The principle scheme of the circadian clock model. The scheme was redrawn from ⁵². Elements of the morning and evening loops of the oscillator are shown in yellow and grey, respectively. Proteins are shown only for EC, ZTL and COP1 for simplicity. Transcriptional regulation is shown by solid lines. EC protein complex formation is denoted by a dashed black line. Post-translational regulation of TOC1 and the EC by GI, ZTL and COP1 are shown by red dashed lines. Acute light responses in gene transcription are shown by flashes. **B.** Cartoon illustrating the role of two factors (timer α and starch level) in regulating starch degradation in the model. Adjustment of starch degradation rate to the duration of the day through: 1) change in the level of timer α – the blue solid line shows acceleration of starch degradation rate in longer days compared to normal days (black line); 2) change in the starch level at dusk – blue dotted lined shows decrease of starch degradation rate in the “early dusk” experiment ⁴⁵. **C.** Scheme of the main fluxes of phosphate in the CBC based on its stoichiometry. The letters on arrows denote: the rate of phosphate flux through the CBC (v , equals half of the rate of CO_2 fixation because 2 molecules of phosphate are transferred in parallel to 1 molecule of CO_2 in the Rubisco carboxylase reaction), the rate of triose-phosphate translocator (TPT) (x or v_{TPT}), sFBPase (y or $v_{TP \rightarrow HP}$) and AGPase (z or $v_{HP \rightarrow St}$) expressed in units of phosphate concentration. The amount of transferred phosphate molecules are shown on the arrows. Dotted lines indicate phosphate fluxes for replenishment of SP. Here, SP corresponds to the

total amount of sugar-phosphates within the CBC, different from F6P, G6P, G1P and ADPG, but include RuBP. TP denote triose-phosphates.

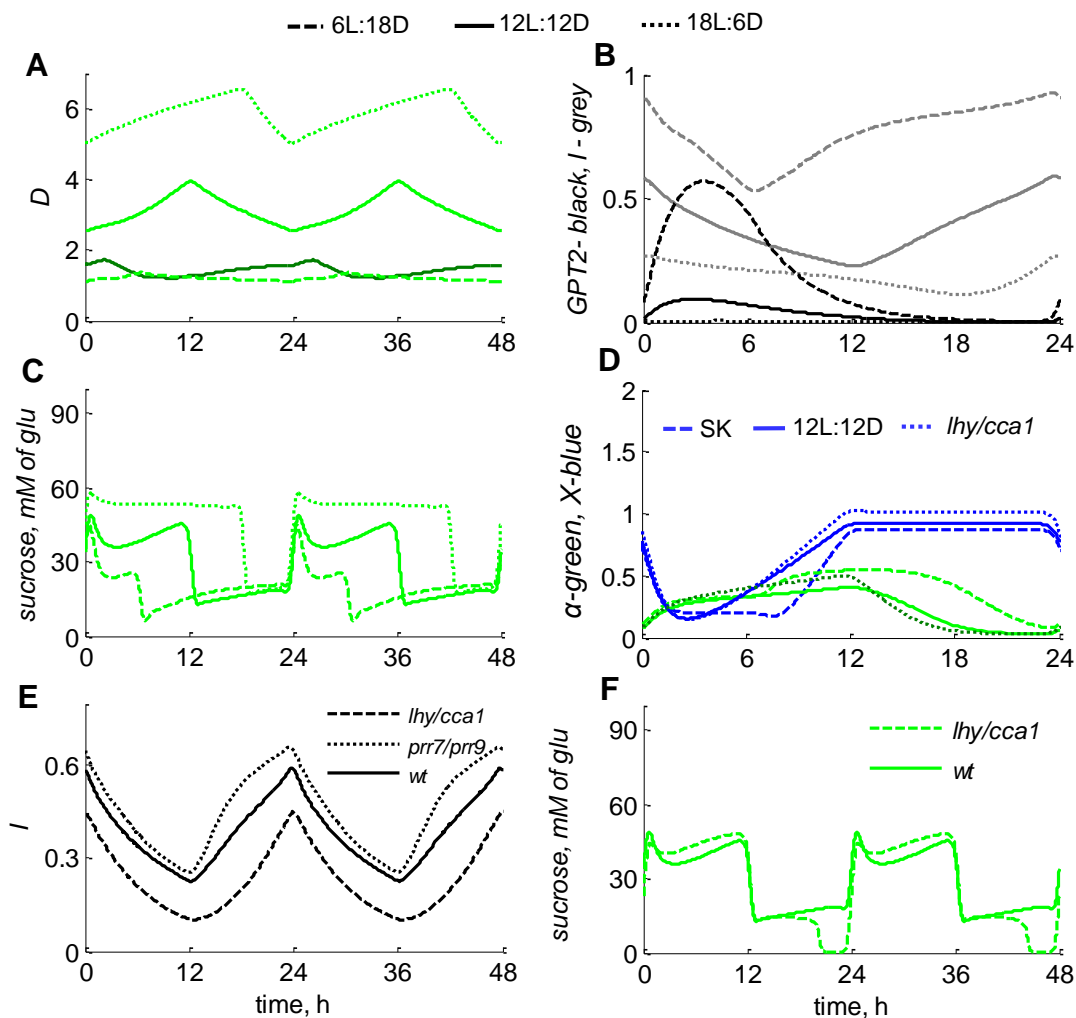


Figure S2. Kinetics of the model components under varying conditions. A. The wild-type kinetics of the sink's demand D (A), I , GPT2 (B) and sucrose (C) levels in source tissues for 6L:18D, 12L:12D and 18L:6D conditions are shown by dashed, solid and dotted lines respectively. The dark green line on A corresponds to D under skeleton photoperiods (2L:5D:5L:12D). Black and grey lines on B correspond to GPT2 and I respectively. D. The profiles of α (green) and X (blue) under 12L:12D (solid lines) and skeleton (dashed lines) photoperiods and in the *lhy/cca1* mutant (dotted lines). E. The profiles of I in the *lhy/cca1* (dashed lines) and *prr7/prr9* (dotted lines) mutants compared to the wild type (solid lines) under 12L:12D. F. Sucrose levels in source tissues of wild type (solid line) and *lhy/cca1* mutant plants (dashed line). Clock mutants were simulated by setting the transcription rates of the corresponding clock genes to 0.

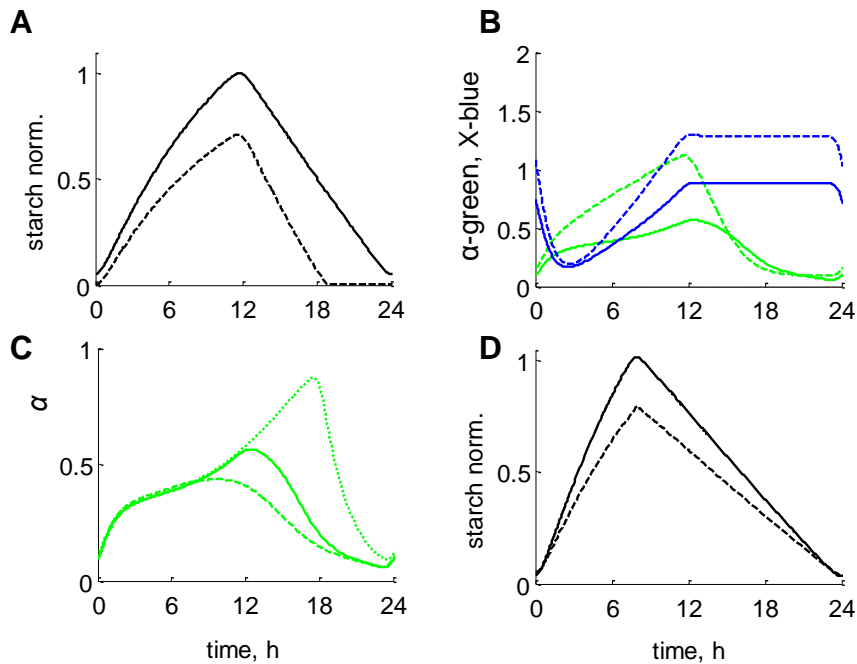


Figure S3. The kinetics of starch (A, D), α (B,C) and X (B) under various conditions in the model without metabolic loop to starch degradation. Simulations were done by omitting the inhibition of starch degradation by I (inhibitory term in equation (22) for X) under the following change in parameters for α : $k_{sa,I}=0.07$. A,B. The profiles of starch (A), α (green) and X (blue) under 12L:12D conditions in wild type (solid lines) and the *lhy/ccal* mutant (dotted lines). C. The profiles of α under 6L:18D, 12L:12D and 18L:6D photoperiods are shown by dashed, solid and dotted lines, respectively. D. Starch profiles in the wild type plants grown under 8L:16D cycle (solid line) and in the “early dusk” experiment (dashed line), where plants grown under 12L:12D photoperiod were suddenly exposed to preliminary darkness at 8ZT, 4h before normal dusk. Starch levels were normalized to the peak level in wild type under 12L:12D cycle

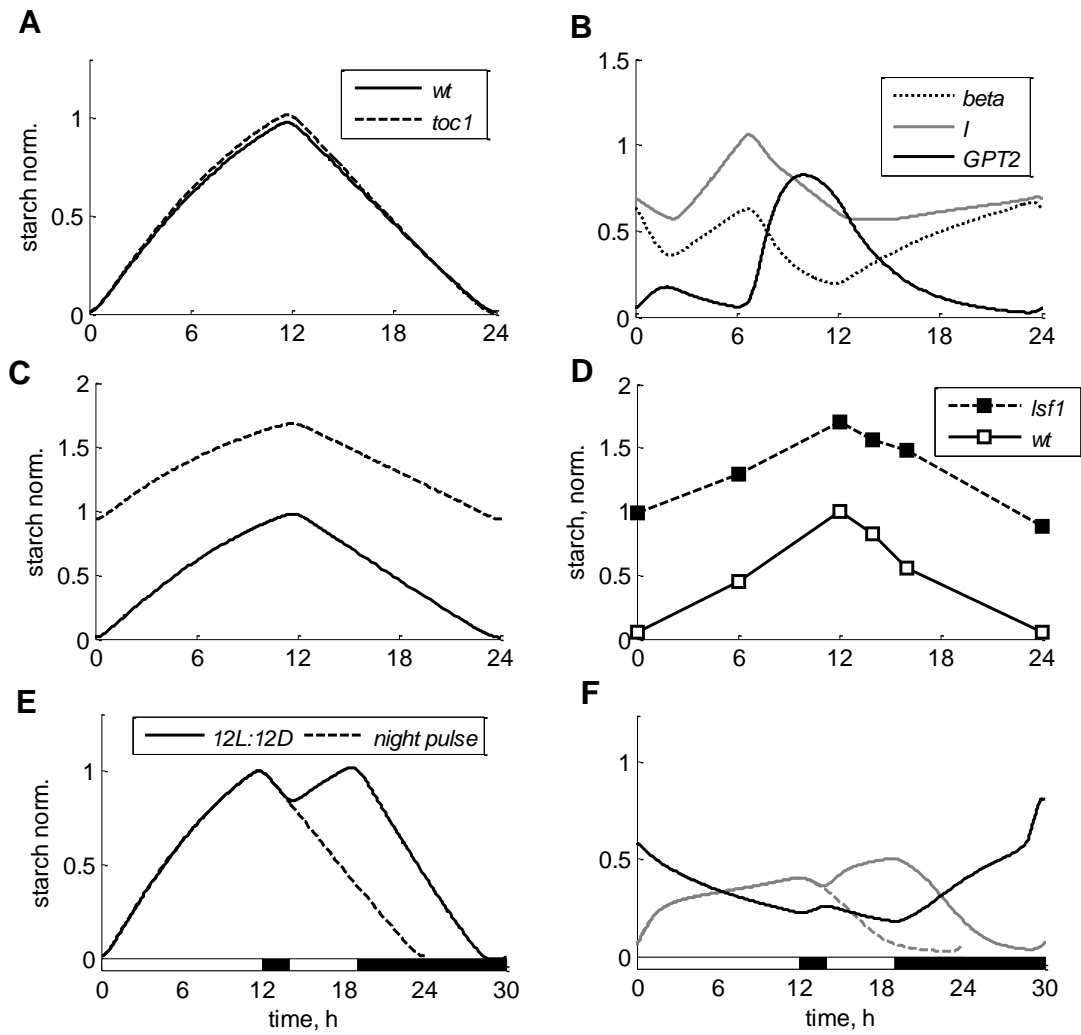


Figure S4. The response of starch metabolism to various genetic perturbations, skeleton photoperiod and “night pulse”. A. Simulated kinetics of starch in the *toc1* mutant (dashed line) compared to wild type (solid line). B. Diurnal profiles of the model components β , I and GPT2 under skeleton photoperiod, represented by black dotted, grey, and black solid lines, respectively. The increase of β during 5h of darkness in the midday results in an increase of I and additional induction of GPT2 after the second period of light. The illumination pattern (2L:5D:5L:12D) corresponds to the one used on Fig. 5 C,D. C, D. Simulated (C) and observed (D) kinetics of the *lsf1* mutant under 12L:12D conditions. The mutant simulations correspond to 60% reduction of the constant k_{SX} . The data were redrawn from ⁴³. E, F. Simulated response of the starch kinetics to the “night pulse” experiment, where an additional 5h period of light was inserted 2h after dusk during the normal dark period in 12L:12D cycle. Starch time course (E) and the kinetics of the diurnal regulators α and I (F) are shown. Dashed lines indicate corresponding time-courses in the normal 12L:12D cycle. White and black bars on the “x”-axis correspond to the periods of light and darkness respectively.

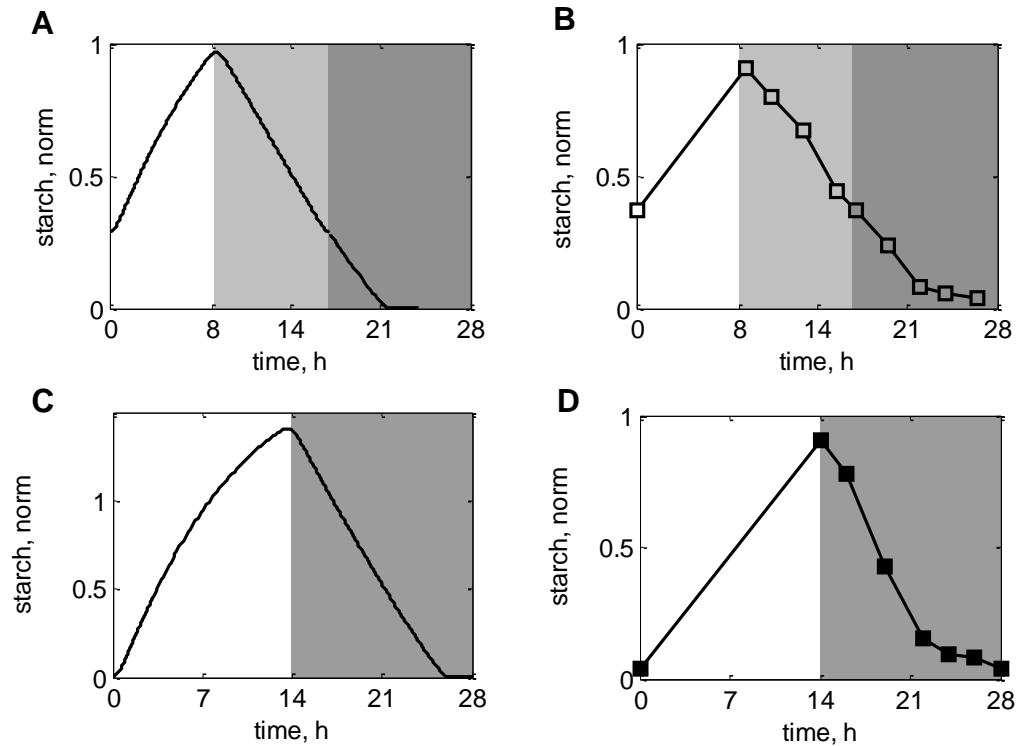


Figure S5. Plants cannot adjust starch degradation rate under T cycles different from 24h. Simulated (A,C) and measured (B,D) kinetics of starch in plants grown under 28h (14L:14D; A,B) and 17h (8.5L:8.5D; C,D) T cycles. C,D: In both simulated and experimental conditions plants were moved into darkness after the last day (shown by dark grey boxes). The experimental plots on panels B, D are redrawn from⁴⁵. Starch levels are normalized to the peak level in 24h T cycles.

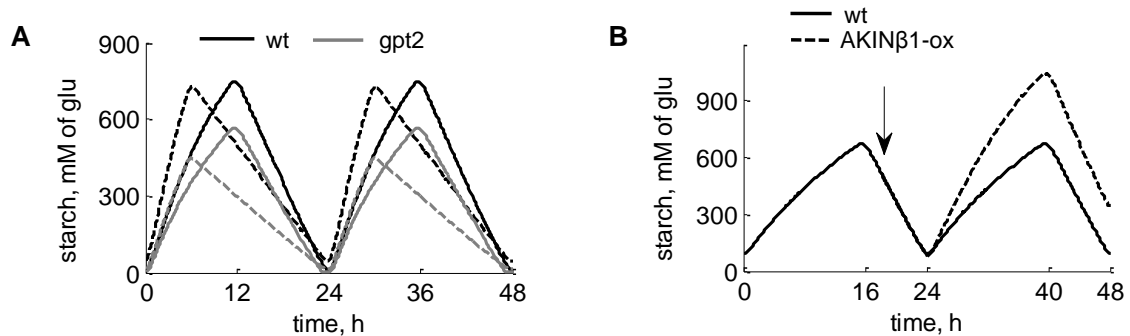


Figure S6. Simulated effects of genetical manipulations of the diurnal regulators on the starch kinetics. A. Mutation of GPT2 reduces starch level in plants under short days. Model simulations of wild type and the *gpt2* mutant are shown by black and grey lines respectively for 12L:12D (solid lines) and 6L:18D (dashed lines) photoperiods. The *gpt2* mutant was simulated by setting the maximal rate of GPT2 (v_{M_GPT2}) to 0. B. Model simulation of starch timecourse in the transient AKIN β 1-overexpressor line (dashed line) under 16L:8D photoperiod. Overexpression of AKIN β 1 was induced at night of the first day, 2 hours after dusk by increasing the rate of AKIN β 1 expression 3-fold (time of induction is shown by arrow). Starch kinetics in the control plant is shown by solid line.

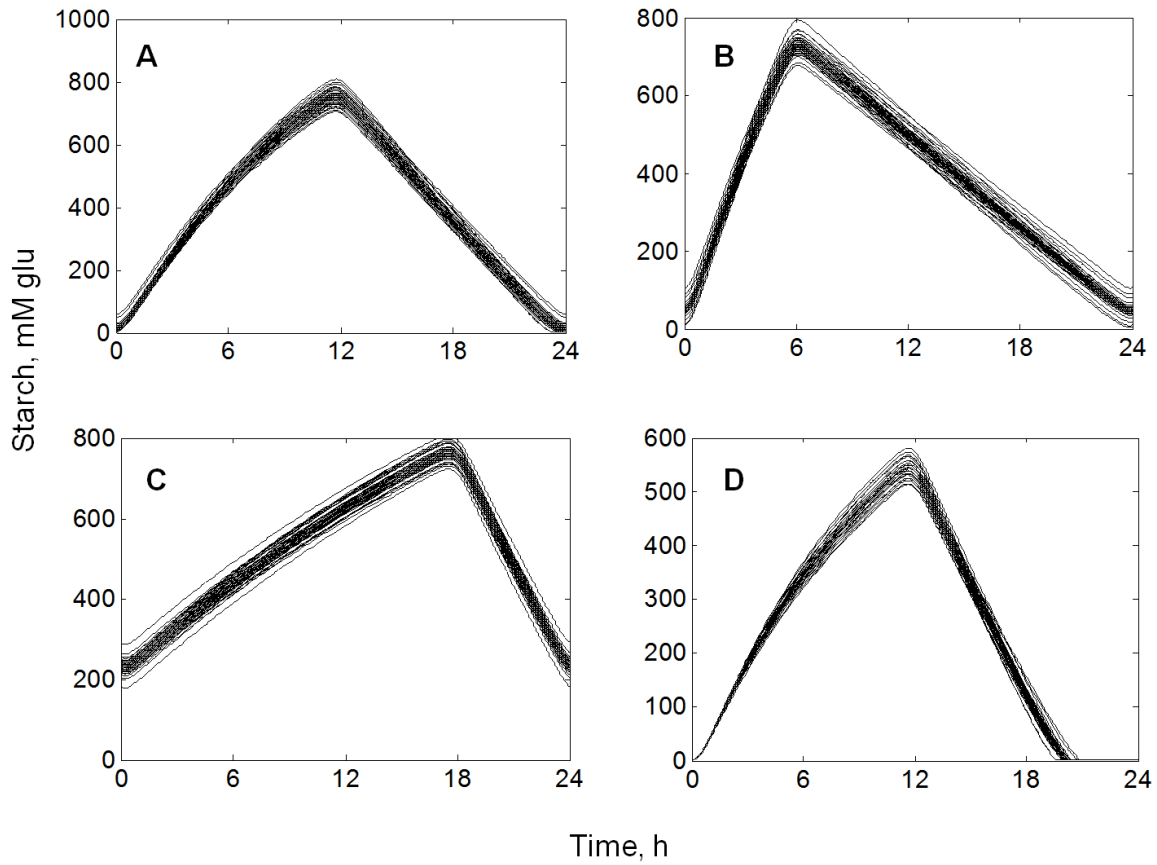


Figure S7. Simulated timecourses of starch under 10% variations of diurnal parameters of equations for I , D , α , β , X , $GPT2$. Simulations were performed for wild type plant grown in 12L:12D, 6L:18D and 18L:6D days (A-C) and for the *lhy/cca1* mutant grown in 12L:12D day. 26 parameters were varied, which are presented in equations (22)-(27), with values from Table S1, part D.